

Binned Cosmic Microwave Background Anisotropy Power Spectra: Peak Location

Silviu Podariu¹, Tarun Souradeep^{1,2}, J. Richard Gott, III³, Bharat Ratra¹,
and Michael S. Vogeley⁴

ABSTRACT

We use weighted mean and median statistics techniques to combine individual cosmic microwave background (CMB) anisotropy detections and determine binned, multipole-space, CMB anisotropy power spectra. The resultant power spectra are peaked. The derived weighted-mean CMB anisotropy power spectrum is not a good representation of the individual measurements in a number of multipole-space bins, if the CMB anisotropy is Gaussian and correlations between individual measurements are small. This could mean that some observational error bars are underestimated, possibly as a consequence of undetected systematic effects. Discarding the most discrepant 5% of the measurements alleviates but does not completely resolve this problem. The median-statistics power spectrum of this culled data set is not as constraining as the weighted-mean power spectrum. Nevertheless it indicates that there is more power at multipoles $\ell \sim 150 - 250$ than is expected in an open cold dark matter (CDM) model, and it is more consistent with a flat CDM model. Unlike the weighted-mean power spectrum, the median-statistics power spectrum at $\ell \sim 400 - 500$ does not exclude a second peak in the flat CDM model.

Subject headings: cosmic microwave background—cosmology: observation—methods: statistical—methods: data analysis—large-scale structure of the universe

1. Introduction

Current observational data favors low-density cosmogonies. The simplest low-density models have either flat spatial hypersurfaces and a constant or time-variable cosmological “constant” Λ

¹Department of Physics, Kansas State University, Manhattan, KS 66506.

²Current address: IUCAA, Post Bag 4, Ganeshkhind, Pune 411007, India.

³Princeton University Observatory, Princeton, NJ 08544.

⁴Department of Physics, Drexel University, Philadelphia, PA 19104.

(see, e.g., Peebles 1984; Peebles & Ratra 1988; Sahni & Starobinsky 2000; Steinhardt 1999; Carroll 2000; Binétruy 2000), or open spatial hypersurfaces and no Λ (see, e.g., Gott 1982, 1997; Ratra & Peebles 1994, 1995; Kamionkowski et al. 1994; Górski et al. 1998). Typically the CMB anisotropy power spectrum is predicted to peak at larger multipole moment ℓ (smaller angular scale) in the open case than in the flat model. This difference in the flat and open model power spectra makes it possible for CMB anisotropy measurements to distinguish between these models. See, e.g., Barreiro (2000), Rocha (1999), Page (1999), and Gawiser & Silk (2000) for recent reviews of the field.

Until very recently no single CMB anisotropy experiment achieved detections over a wide enough range of ℓ space to allow this cosmological test to be performed with data from a single experiment⁵. As a result the test has usually been performed as a goodness-of-fit (χ^2) comparison of CMB anisotropy model predictions and observations (Ganga, Ratra, & Sugiyama 1996)⁶. In this implementation the test favors a flat model over an open one (see, e.g., Dodelson & Knox 2000; Tegmark & Zaldarriaga 2000; Le Dour et al. 2000; Lange et al. 2001; Balbi et al. 2000, 2001; Amendola 2001). However, this χ^2 technique has a number of significant limitations, so these results must be viewed as tentative (see discussion in Ratra et al. 1999b).

Specifically, a χ^2 comparison does not use the complete data from an experiment. Rather, it uses one (or a few) number(s) (the amplitude of a chosen model CMB power spectrum, typically the flat bandpower spectrum) with error bars, as a summary of the complete data of the experiment. However, this amplitude (and error bars) is model dependent. This effect is typically $\sim 10\%$ for a data set with a good detection (see, e.g., Ganga et al. 1997a, 1998; Ratra et al. 1999a), but is not accounted for in the χ^2 comparison. More significantly, the observational error bars are derived from non-Gaussian posterior probability density distribution functions and are thus fairly asymmetric. Since the χ^2 technique assumes symmetric (Gaussian) error bars, the observational error bars must be symmetrized (“Gaussianized”) when this technique is used. This is an arbitrary procedure, and Gaussianizing in different ways leads to different reduced χ^2 values (Ganga et al. 1996). This means that the χ^2 technique can only provide qualitative results. Nevertheless, it is useful, having provided, from a combined analysis of all available early observational results (Ratra et al. 1997), qualitative evidence for more CMB anisotropy power on smaller scales than on larger scales (Ganga et al. 1996), consistent with later observations by single experiments (see, e.g., Netterfield et al. 1997; de Oliveira-Costa et al. 1998; Coble et al. 1999; Miller et al. 1999; Peterson et al. 2000; de Bernardis et al. 2000; Hanany et al. 2000).

Given that current observational error bars are asymmetric (i.e., non-Gaussian), robust results can only be derived from a complete maximum likelihood analysis of a large collection of observa-

⁵The recent BOOMERanG 1998 (de Bernardis et al. 2000) and MAXIMA-1 (Hanany et al. 2000) detections of CMB anisotropy do cover a wide enough range of ℓ space for the test. By including 2σ upper limits on CMB anisotropy (see discussion below), the MAT 1998 (Miller et al. 1999), Viper (Peterson et al. 2000), and BOOMERanG 1997 (Mauskopf et al. 2000) observations also cover a wide enough range of ℓ space.

⁶See Knox & Page (2000) for an alternate approach to this test.

tional data, using realistic model CMB anisotropy power spectra. This is a very time-consuming approach and so has been applied to only a few data sets (see, e.g., Bunn & Sugiyama 1995; Górski et al. 1995; Ganga et al. 1997a, 1997b; Stompor 1997; Ratra et al. 1998; Rocha et al. 1999). Ganga et al. (1997a) generalized the maximum likelihood technique to account for systematic errors (e.g., beamwidth uncertainty, calibration uncertainty). Analyses using this generalized technique have led to significantly revised observational results.

The weighted mean and median statistics techniques are summarized in the next section. In §3 we use these techniques to determine binned CMB anisotropy power spectra using all CMB anisotropy measurements and in §4 we consider a culled collection of good measurements. We conclude in §5.

2. Binned CMB Anisotropy Power Spectra: Techniques

While tight constraints on cosmological parameters will be very valuable, it is also of interest to determine the shape of the observed CMB anisotropy spectrum in a model independent fashion. Since the error bars for experiments to date are large, a tight determination of the CMB anisotropy spectrum is possible only if all available data are used. This approach has been pioneered by Page (1997, 1999).

The data we use in this paper are listed in Table 1 and plotted in Figure 1. We consider all detections at $\ell < 1000$ available as of early November 2000. While we only use detections, defined as those results where the peak of the likelihood function is at least 2σ away from $0\mu\text{K}$, in our analyses here (and these are listed in Table 1), Figure 1 also shows 2σ upper limits. Typically, the bandtemperature (δT_ℓ) values listed in Table 1 have been derived assuming a flat bandpower spectrum and account for known systematic uncertainties (although in most cases only in an approximate manner). Since the flat bandpower spectrum is a more accurate representation of the true spectrum for narrower (in ℓ) window functions, we use observational results for the narrowest windows available. Table 1 lists 142 detections.

To determine the observed CMB anisotropy spectrum, Page (1997, 1999) binned the detections into equally spaced logarithmic bins in ℓ -space, based on the value of ℓ_e , the effective multipole of the experiment’s window function W_ℓ . Here $\ell_e = I(\ell W_\ell)/I(W_\ell)$, where $I(W_\ell) = \sum_{\ell=2}^{\infty} (\ell + 0.5)W_\ell/\{\ell(\ell + 1)\}$. As discussed below, we instead choose to adjust the ℓ -space widths of the bins so as to have approximately the same number of measurements in each bin. Page then Gaussianized the measurements⁷ by defining the error of a measurement, σ , to be half the difference between the upper and lower 1σ values of δT_ℓ for the measurement. The standard expression for the weighted

⁷Bond, Jaffe, & Knox (2000) discuss a more accurate approximation that retains some of the non-Gaussianity.

mean in bin B is

$$\delta T_\ell^B = \frac{\sum_{i=1}^{N_B} (\delta T_\ell)_i / \sigma_i^2}{\sum_{i=1}^{N_B} 1 / \sigma_i^2}, \quad (1)$$

where $i = 1, 2, \dots, N_B$ indexes the N_B measurements in the bin with bandtemperature central values $(\delta T_\ell)_i$ (where the likelihood is at a maximum) and Gaussianized errors σ_i . The (internal) error estimate for each bin is

$$\sigma^B = \left(\sum_{i=1}^{N_B} 1 / \sigma_i^2 \right)^{-1/2}. \quad (2)$$

To plot the observed CMB anisotropy power spectrum, Page places δT_ℓ^B at the arithmetic mean of the ℓ_e values of the measurements that lie in the bin. We choose instead to use the weighted mean of the ℓ_e values,

$$\ell_e^B = \frac{\sum_{i=1}^{N_B} (\ell_e)_i / \sigma_i^2}{\sum_{i=1}^{N_B} 1 / \sigma_i^2}. \quad (3)$$

Since the weighted mean technique assumes Gaussian errors, one may compute a goodness-of-fit parameter, χ_B^2 , for each bin,

$$\chi_B^2 = \frac{1}{N_B - 1} \sum_{i=1}^{N_B} \frac{((\delta T_\ell)_i - \delta T_\ell^B)^2}{\sigma_i^2}. \quad (4)$$

χ_B has expected value unity with error $1/\sqrt{2(N_B - 1)}$, so

$$N_\sigma^B = |\chi_B - 1| \sqrt{2(N_B - 1)} \quad (5)$$

is the number of standard deviations that χ_B deviates from unity. A large value of N_σ^B could indicate the presence of unaccounted-for systematic uncertainties, the invalidity of the Gaussian assumption, or the presence of significant correlations between the measurements.

An alternate method for deriving the observed CMB anisotropy spectrum is the median statistics approach developed by Gott et al. (2001). Here one does not assume that the measurement errors are Gaussian, or even that the magnitudes of the errors are known. One assumes only that the measurements are independent and free of systematic errors. The technique is discussed in detail in Gott et al. (2001). In brief, for each bin in ℓ -space we construct a likelihood function for the true median of the binned measurements⁸ and then integrate over this with a logarithmic prior

⁸As described in Gott et al. (2001), this is a histogram that gives the relative probability of obtaining δT_ℓ . In principle, the highest δT_ℓ -space bin in this histogram extends to $\infty \mu K$; in practice we have picked the width of this bin to be the same as the width of the lowest δT_ℓ -space bin in the histogram. This prescription controls the large δT_ℓ divergence when we integrate over the likelihood function with a logarithmic prior (see below). We have ensured that each ℓ -space bin contains a sufficient number of measurements so that the upper 2σ limit on δT_ℓ^B always lies below the highest δT_ℓ -space bin. Therefore the upper 2σ limit on δT_ℓ^B is insensitive to the procedure used to control the large- δT_ℓ divergence.

to determine the error bars for the bin. We use a logarithmic prior since δT_ℓ is positive definite (see discussion in Gott et al. 2001). We have checked that a linear prior leads to qualitatively similar conclusions, with generally only small quantitative differences. In this case δT_ℓ^B is the median measurement, which is defined to be the mean of the two central measurements if the bin contains an even number of measurements. Since we determine limits on δT_ℓ^B in each ℓ -space bin by integrating the likelihood function for the bin, for accurate 2σ limits we need to ensure that enough measurements lie in each bin. Consequentially, in contrast to Page (1997, 1999), we adjust the widths of the bins so that each of them contain about the same number of measurements, with precise bin membership determined by where breaks occur in the ℓ -space distribution of the measurements of Table 1. And, instead of plotting δT_ℓ^B at the weighted mean of the ℓ_e values of the measurements in the bin, in the median-statistics case we use the median of the ℓ_e values in the bin. Since the median statistics technique ignores the individual measurement errors there is no obvious way of checking the internal goodness of fit of the derived median-statistics CMB anisotropy power spectrum.

3. Binned CMB Anisotropy Power Spectra Using All Measurements

We first consider four different binnings, with about 9, 11, 13, and 16 measurements in each ℓ -space bin. Tables 2 and 3 list results from the weighted-mean and median-statistics analyses. In the median-statistics case, the logarithmic prior makes the integral of the likelihood function diverge at large and at small δT_ℓ . We discuss our prescription for controlling the large- δT_ℓ divergence in footnote 7. To control the small- δT_ℓ divergence we cut off the integral at small δT_ℓ , with the cutoff chosen so that the lower 2σ limit is insensitive to it (see footnote b of Table 3 for the numerical value of the cutoff used). Figures 2 and 3 show the weighted-mean and median-statistics observed CMB anisotropy power spectra.

The weighted mean analysis (Figure 2 and Table 2) results in tight constraints on the observed CMB anisotropy power spectrum, and clearly establishes that it has a peak. For three of the four binnings used this is a rather broad peak⁹, and lies in the interval $\ell \sim 170 - 240$ (for 9 measurements per bin, Figure 2a), $\ell \sim 180 - 210$ (for 11 measurements per bin, Figure 2b), and $\ell \sim 190 - 240$ (for 13 measurements per bin, Figure 2c). For the case of 16 measurements per bin the peak consists of a single bin at $\ell \sim 210$. As expected, the CMB anisotropy power spectrum has less scatter as a function of ℓ when the number of bins is decreased.

We have not considered upper limits in our analyses. From Figure 2 we see that at least four of these are quite constraining and if correct they could significantly affect the shape of the observed power spectrum when accounted for. These are the $\ell = 15, 16,$ and 20 DMR upper limits and the

⁹We define the interval in which the peak lies by the ℓ_e^B values of those bins whose amplitudes are within 90% of the maximum δT_ℓ^B value, for the weighted-mean central value and the $\pm 1\sigma$ and $\pm 2\sigma$ limits.

$\ell = 138.7$ MAX5 μ Pegasi upper limit. The DMR results are derived from the galactic frame maps and ignore the Galactic emission correction (Górski 1997; Górski et al. 1998). Therefore they do not account for the full uncertainty in the DMR data. Our analyses also ignore the correlations between the different DMR ℓ -space results. To derive the MAX5 μ Pegasi upper limit Ganga et al. (1998) marginalized over a possible dust contaminant signal. Ganga et al. (1998) concluded that the MAX5 μ Pegasi upper limit was not inconsistent with the other MAX4 and MAX5 results they studied¹⁰. It is quite possible that knowledge of the dust contaminant signal is less than adequate for the purpose of extracting a robust constraint on the CMB data in this case. It is troubling that three published 2σ upper limits lie at or below the central weighted mean values derived from published detection results.

More worrisome are the large values of N_σ^B (the dashed line in each panel of Figure 2 and the last column of Table 2) for some of the bins. For a Gaussian CMB anisotropy, N_σ^B is a measure of how well the weighted mean and derived bin error bar represents the measurements that lie in the bin. This is larger than 2 (i.e., χ_B is more than 2σ away from what is expected for a Gaussian distribution) for 5 of 16 bins for the 9 measurements per bin case (bin numbers 1, 5, 8, 9, and 15), for 4 of 13 bins for the 11 measurements per bin case (bin numbers 1, 4, 8, and 12, and for bin number 11 $N_\sigma^B = 1.9$), for 3 of 11 bins for the 13 measurements per bin case (bin numbers 1, 7, and 10), and for 3 of 9 bins for the 16 measurements per bin case (bin numbers 1, 5, and 8). Note that $N_\sigma^B < 1.6$ for ℓ -space bins in the peak intervals discussed above (see Table 2).

Since at least two-thirds of the bins have small N_σ^B it is unlikely that the CMB anisotropy is non-Gaussian. The large values of N_σ^B are more likely caused by unaccounted-for foreground contamination, or other effects that lead to underestimated error bars on some of the measurements, and our neglect of correlations between some of the measurements. Since the second effect is thought to be small, the first effect is probably the dominant one. It is important to note that this inconsistency implies that constraints on cosmological parameters derived from χ^2 comparisons of multiple CMB anisotropy observations and model predictions must be interpreted with care.

The median statistics technique does not make use of the error bars on the measurements. Therefore it is ideally suited for an analysis of this combination of CMB anisotropy data. The median statistics analyses result in somewhat weaker constraints on the observed CMB anisotropy detections power spectrum (Figure 3 and Table 3), but still clearly establish that it has a peak. The median-statistics peak interval is slightly broader and extends to slightly smaller angular scales than the weighted-mean peak interval. The median-statistics peak lies in the interval $\ell \sim 160 - 250$ (for 9 measurements per bin, Figure 3a), $\ell \sim 150 - 260$ (for 11 measurements per bin, Figure 3b), $\ell \sim 180 - 240$ (for 13 measurements per bin, Figure 3c), and $\ell \sim 200 - 290$ (for 16 measurements per bin, Figure 3d). It is significant that the median-statistics constraints on δT_ℓ^B are significantly weaker than the weighted-mean constraints on δT_ℓ^B for those bins with large N_σ^B values from the

¹⁰Note from Figure 1 that in the MAX5 μ Pegasi upper limit region of ℓ -space there are a number of detections with low δT_ℓ . These are responsible for the prominent drop in this bin in Figure 2, especially in panels *b* and *c*.

weighted mean analysis. We note that, although the median-statistics constraints are weaker, the median-statistics power spectra of detections are also inconsistent with the three 2σ upper limits that are a problem for the weighted-mean power spectra.

4. Binned CMB Anisotropy Power Spectra Using “Good” Measurements Only

In the weighted mean analyses of the previous section we found that a number of ℓ -space bins had large values of N_σ^B . We argued that these large N_σ^B values were likely the consequence of underestimated error bars on some of the measurements.

To examine this issue we proceed as follows. For each binning in the weighted mean analysis above (i.e., with 9, 11, 13, and 16 measurements per bin) we compute the (“reduced χ^2 ”) contribution to χ_B^2 (eq. [4]) from each measurement in the bin, $\chi_{B,i}^2$, where $\chi_B^2 = \sum_{i=1}^{N_B} \chi_{B,i}^2$. We then list the measurements in decreasing order of $\chi_{B,i}^2$ and discard the first seven that appear in at least 3 of the 4 binnings used. These “discrepant” measurements are listed in Table 4. While this procedure need not necessarily result in reducing all large N_σ^B values, it has the advantage of being less binning dependent than a procedure designed solely to reduce large N_σ^B values to values that are consistent with the Gaussianity assumption.

We first discuss the discrepant measurements of Table 4. As mentioned above, the DMR results do not account for the full uncertainty in the DMR data (Górski 1997; Gorski et al. 1998), and our analyses also ignore correlations between the different DMR ℓ -space measurements. These effects might explain why the DMR measurements in Table 4 are discrepant. The value of the cosmological DMR quadrupole ($\ell = 2$) moment is dependent on the model used to remove foreground Galactic emission (Kogut et al. 1996), and this effect might also contribute to explaining why the DMR $\ell = 2$ moment is discrepant. The low MAX3 μ Pegasi result (Meinhold et al. 1993, as recomputed by J. Gundersen, private communication 1995, see Ratra et al. 1997) is from a region that is contaminated with dust, and this effect could explain why this measurement is discrepant. While the MAT97 Ka2 8-point and Q3 8-point results (Torbet et al. 1999) are higher than neighboring measurements in ℓ -space (see Table 1), we do not know of an effect that might be responsible for making them discrepant. The MSAM 2-beam combined result is from a combined analysis of data from three different flights (Wilson et al. 2000). We note that the three individual MSAM 2-beam results have significant scatter (which seems to be larger than what one might expect from their error bars, see Table 1 of Wilson et al. 2000, unlike the MSAM 3-beam results). It is unclear what causes this scatter, but it is likely that this effect is responsible for placing the MSAM 2-beam measurement among those that are discrepant. We again emphasize that the measurements in Table 4 are discrepant only if the CMB anisotropy is Gaussian. In particular, the posterior probability distribution function of the DMR quadrupole is somewhat non-Gaussian (Hinshaw et al. 1996), and this effect also contributes to explaining this discrepancy.

After removing the seven most discrepant measurements we rebin the remaining 135 measure-

ments, using four different binnings, with about 9, 11, 13, and 15 measurements per ℓ -space bin. We then analyze this culled data set using both the weighted-mean and median-statistics techniques. Tables 5 and 6 and Figures 4 and 5 show the results from these analyses.

The weighted mean analyses (Figure 4 and Table 5) again result in tight constraints on the observed CMB anisotropy power spectrum and again clearly establish the presence of a peak. This is again a rather broad peak that lies in the interval $\ell \sim 170 - 240$ (for 9 measurements per bin, Figure 4a), $\ell \sim 170 - 260$ (for 11 measurements per bin, Figure 4b), $\ell \sim 200 - 250$ (for 13 measurements per bin, Figure 4c), and $\ell \sim 170 - 220$ (for 15 measurements per bin, Figure 4d). After removal of the discrepant measurements of Table 4, the weighted-mean observed CMB anisotropy power spectra have less scatter (compare Figures 4 and 2). There remains the problem of 2σ upper limits that lie below the observed spectrum of the detections, and in particular the $\ell = 138.7$ MAX5 μ Pegasi upper limit is now more inconsistent with the observed spectrum of detections (see Figure 4).

While the culled data results in many fewer large N_σ^B values (the dashed line in each panel of Figure 4 and the last column in Table 5), some bins still contain data that appear to be discrepant (i.e., the weighted mean is more than 2σ away from what is expected for a Gaussian distribution). N_σ^B is larger than 2 for the penultimate of 15 bins for the 9 measurements per bin case, for bin 6 and 11 (of 12) for the 11 measurements per bin case, for the penultimate of 10 bins for the 13 measurements per bin case, and for the penultimate of 9 bins for the 15 measurements per bin case. In the penultimate bins, the most discrepant measurements are SK95 C15 and MAT98 G9 (for 9 measurements per bin), SK95 C15 and MAXIMA-1 4 (for 11 measurements per bin), BOOMERanG98 8 and SK95 C13 (for 13 measurements per bin), and BOOMERanG98 7, SK95 C12 and C13, the last two being equally discrepant (for 15 measurements per bin). The two most discrepant measurements in bin 6 for the 11 measurements per bin case are MAX5 HR5127 6 cm^{-1} and MAT97 Ka2 7-point. It would be useful to understand why these measurements appear discrepant.

While it is possible to remove apparently discrepant measurements from the already culled data set to reduce N_σ^B below 2 for all bins, it is not clear what is gained from this. Clearly, some published CMB anisotropy measurements are mutually inconsistent, if the CMB anisotropy is Gaussian and correlations between measurements are not large. It would thus appear to be dangerous to draw conclusions about the exact position of the peak in the CMB anisotropy spectrum on the basis of the weighted mean analyses alone. Furthermore, χ^2 comparisons between CMB anisotropy measurements and model predictions (to constrain cosmological parameter values) are based on both the above assumptions. Such χ^2 analyses of collections of CMB anisotropy measurements most likely include mutually inconsistent measurements, and so, without more careful investigation, results based on such analyses must be viewed as tentative, at best.

The median statistics results for the culled data set are shown in Figure 5 (also see Table 6). Once again, the median statistics analyses result in somewhat weaker constraints on the observed

CMB anisotropy detections power spectrum than do the weighted mean analyses, but still clearly establish the presence of a peak. The median-statistics peak interval is broader and typically extends more to somewhat smaller angular scales than the weighted-mean peak interval. The median-statistics peak lies in the interval $\ell \sim 150 - 280$ (for 9 measurements per bin, Figure 5a), $\ell \sim 170 - 260$ (for 11 measurements per bin, Figure 5b), $\ell \sim 150 - 240$ (for 13 measurements per bin, Figure 5c), and $\ell \sim 170 - 300$ (for 15 measurements per bin, Figure 5d). The median-statistics power spectra of CMB anisotropy detections are still inconsistent with some of the 2σ upper limits (see Figure 5).

Comparing the median-statistics observed CMB anisotropy detections power spectra to model predictions (Figure 5), we see that the $\Omega_0 = 0.4$ flat- Λ and $\Omega_0 = 1$ fiducial CDM inflation models are not inconsistent with the 2σ range of the observations. While the fiducial CDM model might have slightly lower power than is favored by the observations at $\ell \sim 200$ and at $\ell \sim 400$, the $\Omega_0 = 0.4$ open CDM inflation model has significantly lower power than is indicated by the observations at $\ell \sim 100$ and at $\ell \sim 150 - 250$. We emphasize however that the observations at $\ell \sim 300 - 500$ are quite consistent with the (first peak of the) open model, and the error bars here are large enough for the observations to be consistent with the presence of a second peak in the flat- Λ and fiducial CDM cases. Note that results derived using the weighted mean technique (Figure 4) are inconsistent with these predictions, i.e., at $\ell \sim 300 - 500$ the weighted mean analyses rule out a first peak in the open case and a second peak in the flat models.

5. Conclusions

We extend Page’s (1997, 1999) weighted mean technique and use it to determine the binned observed CMB anisotropy detection power spectrum. Given the observational error bars, the binned power spectra in a number of bins are not a good representation of the measurements. Moreover, there are a number of 2σ upper limits that are inconsistent with the binned power spectra of detections. A number of effects could explain these results, but we suspect that a major one is improperly accounted for or inadequately modelled systematic effects, especially foreground emission contamination, with correlations between some measurements playing a smaller role.

These results have two important ramifications. First, constraints on cosmological parameters derived from χ^2 comparisons between CMB anisotropy model predictions and measurements must be interpreted with great care. And certainly a full maximum likelihood comparison (e.g., Ratra et al. 1999b) is to be preferred. Second, it is important to reanalyze observational data and account for systematic and other effects that may have been ignored in the initial analyses (see Ganga et al. 1997a for the general technique and Ratra et al. 1998, 1999a for cases where a more careful accounting of such effects have led to significant revisions of the observational results).

We have focussed on two methods for dealing with the inconsistencies identified by the weighted mean analyses. We have used the median statistics technique developed by Gott et al. (2001) to

determine an observed CMB anisotropy detections power spectrum. This method makes fewer assumptions than the weighted mean technique (see discussion in Gott et al. 2001). In particular, it completely ignores the error bars on the individual measurements. The median statistics method results in somewhat weaker constraints on the observed CMB anisotropy power spectrum than does the weighted mean technique (compare Figures 3 and 2). If the CMB anisotropy is Gaussian, and if correlations between measurements are small (as is expected for the data we have used), then the weaker median-statistics constraints on the observed CMB anisotropy power spectrum is another indication that the error bars on some measurements might be too small (given the scatter in their central values).

To test the impact of outliers, we remove the seven most discrepant measurements (with largest reduced χ^2 values, as discussed above) and determine a weighted-mean observed CMB anisotropy power spectrum (for the culled data set with 135 measurements). The resultant power spectrum of detections is a much better fit for most (but not all) bins but it is still inconsistent with some of the 2σ upper limits. A median statistics analysis of the culled data set again results in significantly weaker constraints on the observed power spectrum.

In summary, our analyses show that if the CMB anisotropy is Gaussian, and if correlations between measurements are not significant, some observational results are mutually inconsistent. Until this issue is resolved it is not possible to determine a robust observational CMB anisotropy power spectrum, much less constrain cosmological parameters from χ^2 comparisons of theoretical predictions and observational results. While the open CDM model is not inconsistent with observational data at $\ell \sim 300 - 500$, it predicts significantly less power than is seen at $\ell \sim 150 - 250$. If foregrounds do not contribute significantly to the data at $\ell \sim 150 - 250$, the spatially-flat model must be favored significantly over the open one. This result is consistent with other observational data that are compatible with a flat model with a time-variable Λ (see, e.g., Ratra & Peebles 1988; Haiman, Mohr, & Holder 2000; Podariu & Ratra 2000; González-Díaz 2000; Chimento, Jakubi, & Pavoń 2000; Tye & Wasserman 2001; Hebecker & Wetterich 2001; Podariu, Nugent, & Ratra 2001; Barger & Marfatia 2001). Unlike the weighted-mean results, the median-statistics results do not rule out a second peak in the CMB anisotropy at $\ell \sim 400 - 500$.

We acknowledge very valuable discussions with L. Page. We have benefited from the advice and assistance of K. Coble, D. Cottingham, P. de Bernardis, M. Devlin, S. Dicker, K. Ganga, K. Górski, G. Griffin, J. Gundersen, S. Hanany, S. Hancock, E. Leitch, M. Lim, P. Mukherjee, B. Netterfield, L. Piccirillo, S. Platt, D. Pogosyan, G. Rocha, J. Ruhl, R. Stompor, N. Sugiyama, S. Tanaka, E. Torbet, and G. Tucker. SP, BR, and TS acknowledge support from NSF CAREER grant AST-9875031. JRG acknowledges support from NSF grant AST-9900772. MSV acknowledges support from the AAS Small Research Grant program, from John Templeton Foundation grant 938-COS302, and from NSF grant AST-0071201.

Table 1. CMB Anisotropy Detections^a

Experiment	ℓ_e	$\ell_{e-0.5}$ range ^b	δT_ℓ^c (μK)	δT_ℓ (1 σ range) ^d (μK)	Reference ^e
DMR	2.00	2.00–2.00	9.04	6.26–13.2	Górski (1997)
DMR	3.00	3.00–3.00	28.3	23.0–37.1	
DMR	4.00	4.00–4.00	31.4	26.5–39.4	
DMR	5.00	5.00–5.00	27.7	21.7–35.0	
DMR	6.00	6.00–6.00	22.7	18.4–27.9	
DMR	7.00	7.00–7.00	22.1	16.0–29.0	
DMR	8.00	8.00–8.00	23.5	18.7–28.9	
DMR	9.00	9.00–9.00	40.0	34.1–47.0	
DMR	10.0	10.0–10.0	26.2	21.1–32.1	
FIRS	10.8	[2.00]–25.0	31.4	23.4–39.3	Bond (1995)
DMR	11.0	11.0–11.0	40.2	34.0–47.5	
DMR	12.0	12.0–12.0	20.4	13.1–27.4	
DMR	13.0	13.0–13.0	40.1	33.7–47.2	
DMR	14.0	14.0–14.0	32.1	25.8–38.8	
DMR	17.0	17.0–17.0	55.1	47.0–64.0	
DMR	18.0	18.0–18.0	38.3	28.4–48.6	
Tenerife	20.1	14.0–29.0	30.0	18.6–45.3	Gutiérrez et al. (2000)
PyVM1	49.6	28.0–60.0	27.7	22.3–34.0	T. Souradeep pvt. comm. (2000) ^f
BOOM98-1	50.0	26.0–75.0	33.8	28.2–39.0	de Bernardis et al. (2000)
IACBartol	52.7	38.0–77.0	54.6	32.7–81.8	Femenía et al. (1998)
SK94Ka3	55.8	37.0–76.0	51.4	41.2–70.3	Netterfield et al. (1997)
SP94Ka	57.2	35.0–98.0	30.6	21.8–43.5	Ganga et al. (1997a)
BOOM97-1	58.0	25.0–75.0	29.2	17.4–42.1	Mauskopf et al. (2000)
BAM	58.2	16.0–92.0	55.6	40.8–85.2	Tucker et al. (1997)
SK94Q3	59.4	37.0–76.0	41.8	28.4–63.1	
MAT97Ka2-4	63.4	45.0–82.0	35.0	25.3–48.5	Torbet et al. (1999)
MAT97Q1-4	63.4	46.0–82.0	57.0	42.8–75.9	
SK95C3	63.7	37.0–76.0	67.0	50.8–92.7	Netterfield et al. (1997)
SP94Q	66.2	40.0–112.	38.8	28.9–52.7	
SK93	67.0	47.0–95.0	37.1	27.0–50.1	Netterfield et al. (1997)
PyVM2	73.5	48.0–100.	30.8	24.2–38.3	
SK94Ka4	76.5	57.0–96.0	33.1	25.5–46.8	

Table 1—Continued

Experiment	ℓ_e	$\ell_{e-0.5}$ range ^b	δT_ℓ^c	δT_ℓ (1 σ range) ^d	Reference ^e
MAXIMA1-1	77.0	36.0–110.	44.7	38.3–52.0	Hanany et al. (2000)
MAT97Q3-5	82.7	63.0–100.	47.0	33.2–64.6	
SK95C4	83.0	54.0–96.0	39.1	29.8–56.2	
QMAP1Q	83.7	43.0–146.	47.0	35.5–56.8	Devlin et al. (1998)
MAT97Ka2-5	86.5	65.0–103.	52.0	42.5–64.2	
MAT97Q1-5	86.7	65.0–104.	40.0	25.4–54.6	
PyIII	87.7	52.0–98.0	63.7	49.4–84.5	Rocha et al. (1999)
QMAP2Ka1	91.1	60.0–165.	44.9	32.0–56.1	Herbig et al. (1998)
PyI+II	91.7	53.0–99.0	52.1	39.0–71.6	Rocha et al. (1999)
QMAP1Ka	92.0	56.0–159.	47.9	39.2–55.8	
SK94Ka5	96.0	76.0–116.	45.1	34.6–63.4	
ARGO Herc.	97.6	60.0–168.	32.6	28.0–37.9	Ratra et al. (1999a)
BOOM98-2	100.	76.0–125.	55.8	48.5–62.8	
BOOM97-2	102.	76.0–125.	48.8	39.2–58.9	
MAT97Q3-6	106.	84.0–121.	61.0	46.6–80.0	
JB-IAC-L	106.	90.0–129.	43.0	30.7–55.8	Dicker et al. (1999)
MAT97Ka2-6	107.	86.0–124.	71.0	58.7–84.9	
SK95C5	108.	76.0–115.	55.6	43.6–76.1	
PyVM3	108.	81.0–131.	33.5	26.2–41.7	
Viper1	108.	46.0–135.	61.0	38.5–92.4	Peterson et al. (2000)
MAT97Q1-6	110.	87.0–126.	56.0	41.9–71.1	
MAX4 6/cm γ UM	114.	70.0–196.	41.6	29.2–60.3	S. Tanaka pvt. comm. (1995)
MAX4 6/cm ι D	114.	70.0–196.	67.5	37.6–112.	Ganga et al. (1998)
MAX4 9/cm γ UM	114.	70.0–196.	53.6	37.0–79.2	S. Tanaka pvt. comm. (1995)
MAX4 9/cm σ H	114.	70.0–196.	53.0	29.6–90.7	Ganga et al. (1998)
SK94Ka6	115.	95.0–136.	34.3	22.8–50.9	
QMAP2Q	125.	76.0–228.	56.0	47.4–63.9	
MAT97Q3-7	125.	103.–141.	72.0	58.0–89.6	
MAT97Ka2-7	127.	106.–145.	93.0	76.2–111.	
MAT98G6	129.	96.0–153.	55.0	37.4–73.5	Miller et al. (1999)
MAT97Q1-7	131.	107.–147.	81.0	63.1–102.	
MAX4 3.5/cm γ UM	133.	80.0–224.	78.6	56.3–108.	S. Tanaka pvt. comm. (1995)
MAX4 3.5/cm σ H	133.	80.0–224.	85.8	58.4–129.	Ganga et al. (1998)

Table 1—Continued

Experiment	ℓ_e	$\ell_{e-0.5}$ range ^b	δT_ℓ ^c	δT_ℓ (1 σ range) ^d	Reference ^e
MAX4 3.5/cm ι D	133.	80.0–224.	56.6	37.4–86.4	Ganga et al. (1998)
MAX5 6/cm HR	133.	80.0–224.	26.7	19.7–37.1	Ganga et al. (1998)
MAX5 6/cm ϕ H	133.	80.0–224.	73.8	55.9–99.4	Ganga et al. (1998)
MAX5 9/cm HR	133.	80.0–224.	37.0	24.6–54.6	Ganga et al. (1998)
SK95C6	135.	97.0–141.	65.9	52.5–85.8	
MAX5 3.5/cm HR	139.	83.0–232.	40.0	27.5–58.0	Ganga et al. (1998)
MAX5 3.5/cm ϕ H	139.	83.0–232.	50.5	32.0–77.2	Ganga et al. (1998)
PyVM4	141.	113.–161.	37.8	26.8–49.3	
MAX3 γ UM	142.	85.0–240.	74.2	59.8–96.1	J. Gundersen pvt. comm. (1995)
MAX3 μ Peg	144.	86.0–243.	23.4	16.2–36.0	J. Gundersen pvt. comm. (1995)
MAT97Ka2-8	145.	126.–165.	103.	86.4–121.	
QMAP2Ka2	145.	141.–224.	62.2	48.2–74.6	
MAT97Q3-8	145.	122.–161.	115.	96.1–137.	
MAXIMA1-2	147.	111.–185.	54.4	48.7–60.7	
BOOM98-3	150.	126.–175.	64.5	56.5–72.2	
MAT97Q1-8	151.	127.–167.	86.0	67.0–107.	
BOOM97-3	153.	126.–175.	67.2	56.6–78.2	
MAT98G7	155.	117.–183.	82.0	69.2–94.8	
SK95C7	158.	119.–165.	74.2	59.4–95.4	
MSAM 2beam comb.	159.	83.0–234.	47.0	41.5–52.5	Wilson et al. (2000)
MAT97Q3-9	165.	141.–180.	72.0	49.8–97.1	
MAT97Ka2-9	166.	145.–184.	65.0	46.8–82.3	
SK95R3	170.	115.–236.	60.8	49.3–73.9	
PyIIIS	171.	128.–230.	65.7	51.4–86.6	Rocha et al. (1999)
PyVM5	172.	145.–192.	58.4	41.4–75.9	
MAT97Q1-9	172.	147.–188.	93.0	68.2–118.	
Viper2	173.	92.0–193.	77.0	56.1–104.	
SK94Q9	176.	153.–195.	142.	94.5–204.	
SK95C8	178.	140.–184.	83.4	68.0–106.	
MAT97Ka2-10	182.	165.–204.	67.0	43.0–88.1	
MAT97Q3-10	184.	161.–200.	87.0	66.1–108.	
MAT97Q3-11	196.	180.–219.	90.0	62.5–119.	
SK95C9	197.	159.–204.	78.3	62.4–101.	

Table 1—Continued

Experiment	ℓ_e	$\ell_{e-0.5}$ range ^b	δT_ℓ ^c	δT_ℓ (1 σ range) ^d	Reference ^e
BOOM98-4	200.	176.–225.	68.6	60.3–76.7	
PyVM6	203.	176.–223.	95.4	68.8–123.	
BOOM97-4	204.	176.–225.	71.9	60.5–83.3	
JB-IAC-S	207.	190.–227.	63.0	55.7–71.1	Harrison et al. (2000)
MAT97Q3-12	212.	199.–238.	100.	71.2–131.	
MAT97Ka2-12	215.	204.–243.	128.	92.6–161.	
SK95C10	217.	178.–222.	78.3	59.7–103.	
MAXIMA1-3	223.	186.–260.	77.9	71.1–85.1	
SK95R4	234.	182.–301.	80.3	65.2–99.	
SK95C11	237.	199.–244.	85.5	67.4–110.	
Viper3	237.	148.–283.	65.0	47.2–89.6	
MAT98G8	248.	185.–302.	83.0	72.6–92.7	
BOOM98-5	250.	226.–275.	65.6	57.7–73.4	
BOOM97-5	255.	226.–275.	60.8	48.0–73.1	
SK95C12	257.	221.–265.	115.	92.9–146.	
MAT97Q3-14	258.	236.–277.	119.	79.2–157.	
Viper4	263.	157.–441.	79.0	63.6–98.1	
MSAM 3beam comb.	263.	181.–375.	53.0	47.3–58.7	Wilson et al. (2000)
SK95C13	277.	241.–286.	119.	94.9–151.	
SK95R5	286.	247.–365.	71.1	48.1–93.1	
SK95C14	297.	263.–307.	76.2	50.1–104.	
MAXIMA1-4	300.	261.–335.	61.0	55.7–66.5	
BOOM98-6	300.	276.–325.	51.4	45.0–57.7	
BOOM97-6	305.	276.–325.	55.4	38.6–69.7	
SK95C15	316.	282.–326.	128.	97.4–166.	
MAT98G9	319.	267.–347.	70.0	57.7–81.5	
SK95C16	334.	301.–345.	113.	72.2–154.	
BOOM98-7	350.	326.–375.	39.4	34.0–44.7	
MAXIMA1-5	374.	336.–410.	47.6	43.4–52.1	
CAT1 (Yr. 1)	396.	351.–471.	51.8	37.9–65.7	G. Rocha pvt. comm. (1997)
CAT1 (Yr. 2)	396.	351.–471.	56.6	42.6–69.6	Baker et al. (1999)
BOOM98-8	400.	376.–425.	36.2	30.7–41.4	
MAXIMA1-6	447.	411.–485.	39.1	35.1–43.3	

Table 1—Continued

Experiment	ℓ_e	$\ell_{e-0.5}$ range ^b	δT_ℓ ^c	δT_ℓ (1 σ range) ^d	Reference ^e
BOOM98-9	450.	426.–475.	36.8	30.8–42.5	
BOOM98-10	500.	476.–525.	38.0	31.2–44.2	
MAXIMA1-7	522.	486.–560.	48.4	43.6–53.3	
BOOM98-11	550.	526.–575.	41.8	33.9–49.0	
Viper6	588.	443.–794.	65.0	39.5–90.5	
MAXIMA1-8	597.	561.–635.	39.1	34.1–44.2	
OVRO	599.	361.–754.	59.0	52.5–67.6	Leitch et al. (2000)
BOOM98-12	600.	576.–625.	39.2	30.0–47.2	
CAT2 (Yr. 1)	608.	565.–710.	49.1	35.2–68.3	G. Rocha pvt. comm. (1997)
MAXIMA1-9	671.	636.–710.	42.8	36.7–48.8	
MAXIMA1-10	742.	711.–785.	46.7	38.9–54.4	

^aWhere known, beamwidth and calibration uncertainties have been accounted for and foreground contamination removed.

^bThe two values of ℓ where $W_{\ell_{e-0.5}} = e^{-0.5}W_{\ell_m}$, where ℓ_m is the value of ℓ where W_ℓ is largest.

^cBandtemperature central value (this is where the likelihood is largest), typically derived assuming a flat bandpower spectrum.

^d1 σ range of band temperature. Accounts for known systematic uncertainties.

^eTypically provided only the first time the experiment appears in the Table.

^fIgnores cross-modulation correlations.

Table 2. Weighted Mean Results Using All Measurements

Bin	ℓ_e^B ^a	N^B	δT_ℓ^B (μK)	δT_ℓ^B (1σ range) (μK)	δT_ℓ^B (2σ range) (μK)	N_σ^B
9 measurements per bin						
1	4.97	8	21.8	19.9–23.7	18.0–25.6	3.39
2	12.8	9	33.8	31.4–36.3	28.9–38.7	1.29
3	52.0	8	33.3	29.9–36.6	26.6–39.9	.691
4	71.8	8	38.9	35.3–42.4	31.7–46.0	.432
5	87.8	9	47.6	43.5–51.7	39.5–55.7	2.09
6	102.	10	43.3	40.3–46.3	37.4–49.3	1.46
7	119.	8	53.1	47.9–58.4	42.7–63.6	.885
8	132.	10	51.9	46.6–57.1	41.4–62.3	2.26
9	145.	9	52.8	48.9–56.7	45.0–60.6	3.83
10	156.	8	59.8	56.2–63.5	52.5–67.2	1.14
11	174.	9	71.3	64.8–77.7	58.3–84.2	.882
12	204.	9	71.2	66.7–75.8	62.2–80.3	.408
13	240.	9	75.0	71.1–79.0	67.1–83.0	.0803
14	287.	8	57.7	54.6–60.9	51.5–64.0	.529
15	402.	10	42.5	40.5–44.6	38.4–46.7	2.19
16	588.	10	44.4	42.2–46.6	39.9–48.8	.285
11 measurements per bin						
1	6.09	11	23.8	22.1–25.5	20.4–27.2	3.72
2	29.8	10	34.4	31.9–36.8	29.4–39.3	1.10
3	68.9	12	37.9	34.8–41.1	31.6–44.3	.897
4	88.4	10	47.4	43.5–51.3	39.6–55.2	2.32
5	102.	10	43.8	40.8–46.8	37.8–49.7	1.58
6	123.	10	58.0	53.1–63.0	48.2–67.9	.337
7	137.	12	40.7	36.4–45.0	32.1–49.2	1.33
8	153.	12	61.0	58.1–64.0	55.1–67.0	2.51
9	177.	11	72.8	66.8–78.8	60.8–84.8	1.19
10	213.	11	73.2	69.5–76.9	65.8–80.6	.645

Table 2—Continued

Bin	ℓ_e^B ^a	N^B	δT_ℓ^B	δT_ℓ^B (1σ range)	δT_ℓ^B (2σ range)	N_σ^B
11	277.	12	61.7	59.0–64.5	56.2–67.2	1.88
12	400.	11	42.8	40.7–44.8	38.6–46.9	2.07
13	588.	10	44.4	42.2–46.6	39.9–48.8	.285
13 measurements per bin						
1	6.09	11	23.8	22.1–25.5	20.4–27.2	3.72
2	32.4	13	34.2	31.9–36.6	29.6–38.9	.670
3	73.5	12	40.0	36.9–43.2	33.7–46.3	1.16
4	96.3	12	44.7	41.8–47.5	39.0–50.3	.123
5	116.	14	52.2	48.4–56.0	44.7–59.7	.870
6	136.	12	46.7	42.1–51.3	37.5–55.9	1.28
7	152.	13	58.0	55.1–60.8	52.3–63.7	3.94
8	188.	14	72.0	67.7–76.4	63.3–80.8	1.55
9	241.	15	68.3	65.4–71.2	62.5–74.1	1.51
10	349.	14	49.6	47.4–51.7	45.2–53.9	3.09
11	546.	12	42.6	40.7–44.4	38.9–46.3	.181
16 measurements per bin						
1	7.89	17	26.3	24.8–27.8	23.3–29.3	4.79
2	57.8	14	34.7	32.0–37.3	29.3–40.0	.742
3	90.7	15	43.7	41.3–46.2	38.8–48.7	.413
4	113.	14	49.9	46.2–53.6	42.5–57.2	.0767
5	138.	18	51.8	48.1–55.4	44.5–59.1	4.33
6	156.	14	59.5	56.5–62.4	53.6–65.3	.401
7	210.	17	74.4	71.0–77.9	67.6–81.3	1.19
8	294.	17	58.0	55.7–60.4	53.3–62.7	3.57
9	505.	16	43.0	41.4–44.6	39.8–46.2	.111

^aWeighted mean of ℓ_e values of measurements in the bin.

Table 3. Median Statistics Results Using All Measurements

Bin	ℓ_e^B ^a	N^B	δT_ℓ^B (μK)	δT_ℓ^B (1 σ range) (μK)	δT_ℓ^B (2 σ range) (μK)
9 measurements per bin ^b					
1	5.50	8	24.7	22.6–28.1	11.4–31.9
2	13.0	9	31.9	30.3–39.0	24.2–40.2
3	56.5	8	35.2	30.2–48.1	28.1–54.6
4	66.6	8	37.6	34.8–43.1	31.5–56.8
5	86.7	9	47.0	45.6–49.8	39.9–52.1
6	106.	10	50.7	44.3–55.8	34.2–61.0
7	114.	8	54.5	50.7–56.0	35.8–68.1
8	133.	10	67.6	55.8–78.1	35.6–83.7
9	144.	9	53.0	41.0–64.3	29.3–93.2
10	156.	8	68.9	64.9–73.8	50.4–82.8
11	173.	9	74.8	66.0–84.8	60.1–91.9
12	204.	9	78.3	73.6–92.1	67.0–99.3
13	248.	9	79.9	68.5–84.0	63.8–109.
14	292.	8	63.6	55.0–75.0	51.8–79.0
15	385.	10	48.4	39.3–55.5	37.1–78.3
16	598.	10	44.2	41.1–48.3	39.1–54.6
11 measurements per bin ^b					
1	7.00	11	27.4	23.8–29.9	22.3–32.0
2	19.1	10	34.9	31.2–39.9	27.8–52.9
3	63.6	12	37.6	34.0–41.9	30.7–52.8
4	87.2	10	47.0	45.1–47.9	40.7–52.1
5	107.	10	55.7	46.2–56.0	33.7–61.0
6	120.	10	55.3	53.4–66.0	42.0–76.6
7	134.	12	50.9	38.5–64.7	32.2–74.1
8	152.	12	68.8	64.8–74.8	61.3–85.2
9	176.	11	78.1	68.2–85.5	62.7–90.5
10	215.	11	78.2	72.8–83.3	66.5–96.0

Table 3—Continued

Bin	ℓ_e^B ^a	N^B	δT_ℓ^B	δT_ℓ^B (1 σ range)	δT_ℓ^B (2 σ range)
11	263.	12	72.5	63.2–79.1	59.5–106.
12	374.	11	50.6	39.8–56.0	37.6–68.8
13	598.	10	44.2	41.1–48.3	39.1–54.6
13 measurements per bin ^b					
1	7.00	11	27.4	23.8–29.9	22.3–32.0
2	49.6	13	33.3	30.6–39.3	29.3–52.4
3	70.3	12	40.1	38.0–44.9	34.8–47.0
4	94.0	12	48.2	45.0–52.0	42.8–55.2
5	114.	14	55.8	54.3–57.4	46.8–67.5
6	133.	12	57.6	42.8–73.3	37.5–77.6
7	151.	13	66.8	64.5–73.5	55.4–83.9
8	180.	14	77.4	69.9–84.4	66.4–90.2
9	237.	15	78.9	76.0–82.5	65.0–95.6
10	317.	14	57.7	53.1–70.1	49.4–75.7
11	592.	12	42.2	39.2–46.9	39.1–49.0
16 measurements per bin ^b					
1	10.0	17	29.7	27.2–31.4	23.2–37.6
2	58.8	14	37.5	34.2–42.5	30.7–54.4
3	87.7	15	46.8	44.9–47.8	40.2–51.4
4	112.	14	55.8	53.3–57.5	42.2–61.5
5	134.	18	62.8	55.0–73.9	39.6–79.9
6	162.	14	66.3	64.7–72.6	59.8–77.3
7	204.	17	80.1	78.2–85.4	71.0–89.9
8	286.	17	70.8	64.0–78.5	58.7–106.
9	536.	16	44.0	40.0–47.9	39.1–50.2

^aMedian of ℓ_e values of measurements in the bin.

^bThe lower cutoffs on the integral of the likelihood function are 4, 1, 1, and 1 μK for 9, 11, 13, and 16 measurements per bin.

Table 4. Discrepant Measurements

Measurement	ℓ	$\chi^2_{B,i}(9)^a$	$\chi^2_{B,i}(11)^a$	$\chi^2_{B,i}(13)^a$	$\chi^2_{B,i}(16)^a$
DMR	2.00	1.9	1.8	1.8	1.5
DMR	9.00	1.1	.64	.64	.29
DMR	17.0	.79	.66	.50	.72
MAX3 μ Peg	144.	1.1	.27	1.0	.48
MAT97Ka2-8	145.	1.0	.53	.56	.51
MAT97Q3-8	145.	1.1	.63	.64	.56
MSAM 2beam comb.	159.	.77	.59	.33	.39

^aReduced χ^2 of the measurement for the case with 9, 11, 13, and 16 measurements per bin, respectively.

Table 5. Weighted Mean Results Using “Good” Measurements Only

Bin	ℓ_e^B ^a	N^B	δT_ℓ^B (μK)	δT_ℓ^B (1 σ range) (μK)	δT_ℓ^B (2 σ range) (μK)	N_σ^B
9 measurements per bin						
1	7.18	9	27.2	25.1–29.2	23.1–31.2	.394
2	30.2	8	31.8	29.2–34.5	26.6–37.1	.275
3	59.6	8	40.7	35.6–45.8	30.5–50.9	.417
4	75.7	8	38.9	35.5–42.4	32.0–45.8	1.20
5	94.9	9	43.8	40.7–46.9	37.7–49.9	.550
6	107.	8	48.0	43.6–52.3	39.3–56.7	.293
7	122.	9	56.4	51.3–61.5	46.2–66.6	.237
8	134.	10	46.3	41.0–51.5	35.8–56.8	1.21
9	148.	9	61.3	57.8–64.8	54.2–68.3	.749
10	171.	9	69.4	63.0–75.8	56.6–82.1	1.07
11	202.	9	70.5	66.0–75.0	61.6–79.4	1.13
12	238.	9	74.5	70.6–78.5	66.6–82.4	.388
13	287.	10	58.9	55.8–62.0	52.7–65.1	1.45
14	402.	10	42.5	40.5–44.6	38.4–46.7	2.19
15	588.	10	44.4	42.2–46.6	39.9–48.8	.285
11 measurements per bin						
1	7.96	11	27.7	25.8–29.6	24.0–31.4	.225
2	41.1	11	33.3	30.5–36.1	27.7–38.8	1.31
3	74.0	11	40.0	36.8–43.2	33.5–46.4	.947
4	96.3	12	44.7	41.8–47.5	39.0–50.3	.123
5	110.	10	46.1	41.4–50.7	36.7–55.4	.0751
6	130.	12	54.4	50.2–58.7	45.9–63.0	2.04
7	148.	11	60.0	56.6–63.4	53.2–66.8	.688
8	172.	11	70.6	64.7–76.5	58.9–82.4	1.32
9	211.	11	73.6	69.9–77.3	66.2–81.0	.661
10	257.	11	65.9	62.3–69.5	58.7–73.1	1.63
11	350.	12	48.9	46.7–51.1	44.5–53.3	2.59

Table 5—Continued

Bin	ℓ_e^B ^a	N^B	δT_ℓ^B	δT_ℓ^B (1 σ range)	δT_ℓ^B (2 σ range)	N_σ^B
12	546.	12	42.6	40.7–44.4	38.9–46.3	.181
13 measurements per bin						
1	8.92	14	28.4	26.6–30.1	24.9–31.9	.104
2	55.1	13	35.3	32.4–38.2	29.5–41.1	.624
3	86.6	14	40.2	37.7–42.8	35.2–45.3	.563
4	106.	14	49.0	45.6–52.4	42.2–55.9	.469
5	131.	14	53.3	49.3–57.3	45.2–61.4	1.75
6	152.	13	61.7	58.5–65.0	55.2–68.2	.0879
7	197.	13	71.1	67.0–75.2	62.8–79.3	1.25
8	247.	14	69.2	66.1–72.4	63.0–75.5	1.62
9	349.	14	49.6	47.4–51.7	45.2–53.9	3.09
10	546.	12	42.6	40.7–44.4	38.9–46.3	.181
15 measurements per bin						
1	8.92	14	28.4	26.6–30.1	24.9–31.9	.104
2	61.2	16	35.9	33.4–38.3	31.0–40.7	.693
3	94.7	15	44.6	42.0–47.3	39.4–49.9	.427
4	116.	15	53.3	49.6–56.9	45.9–60.6	1.03
5	142.	15	52.9	49.6–56.1	46.4–59.3	1.49
6	166.	14	71.7	67.1–76.3	62.4–81.0	1.68
7	224.	16	72.6	69.6–75.6	66.5–78.6	.879
8	322.	15	53.4	51.1–55.6	48.9–57.8	3.27
9	526.	15	42.3	40.5–44.0	38.8–45.7	.177

^aWeighted mean of ℓ_e values of measurements in the bin.

Table 6. Median Statistics Results Using “Good” Measurements Only

Bin	ℓ_e^B ^a	N^B	δT_ℓ^B (μK)	δT_ℓ^B (1 σ range) (μK)	δT_ℓ^B (2 σ range) (μK)
9 measurements per bin ^b					
1	7.00	9	27.4	24.2–29.6	22.6–31.4
2	19.1	8	32.6	29.6–37.3	22.0–40.8
3	58.8	8	43.4	33.5–54.4	29.4–57.6
4	76.7	8	38.9	36.6–43.7	31.4–47.0
5	91.7	9	47.5	45.0–52.0	37.5–55.3
6	108.	8	55.7	47.4–60.1	35.0–62.9
7	115.	9	54.8	53.2–60.2	38.4–71.2
8	133.	10	57.9	44.4–72.4	37.0–79.8
9	150.	9	66.7	62.7–74.2	46.0–81.0
10	172.	9	70.8	65.2–79.5	60.1–91.1
11	200.	9	77.0	69.5–88.2	65.9–94.7
12	237.	9	78.2	68.7–81.6	63.8–85.1
13	282.	10	72.2	58.5–78.5	53.2–117.
14	385.	10	48.4	39.3–55.5	37.1–78.2
15	598.	10	44.2	41.1–48.3	39.1–54.6
11 measurements per bin ^b					
1	8.00	11	27.4	23.8–29.9	22.3–32.0
2	52.7	11	33.4	30.8–39.9	29.5–51.2
3	73.5	11	39.1	37.3–46.0	33.8–47.9
4	94.0	12	48.2	45.0–52.0	42.7–55.2
5	112.	10	54.3	47.6–56.0	34.2–64.7
6	133.	12	67.4	56.3–74.0	46.3–80.6
7	147.	11	64.0	54.9–70.9	42.3–75.3
8	172.	11	71.1	65.9–80.5	62.4–87.7
9	207.	11	78.3	78.0–85.9	69.9–96.1
10	257.	11	77.1	66.2–84.2	62.2–115.
11	326.	12	55.8	51.6–61.0	45.6–74.5

Table 6—Continued

Bin	ℓ_e^B ^a	N^B	δT_ℓ^B	δT_ℓ^B (1σ range)	δT_ℓ^B (2σ range)
12	592.	12	42.2	39.2–46.9	39.1–49.0
13 measurements per bin ^b					
1	10.4	14	28.8	26.7–31.4	23.1–32.1
2	58.2	13	38.3	35.0–47.0	31.0–55.0
3	86.6	14	45.0	41.9–47.0	35.9–48.4
4	108.	14	54.4	50.4–55.8	42.2–61.0
5	133.	14	58.7	55.3–72.3	43.6–78.5
6	153.	13	65.6	64.5–70.7	61.1–74.2
7	184.	13	78.1	72.1–86.0	67.3–91.6
8	243.	14	79.5	78.1–83.7	65.3–99.5
9	317.	14	57.7	53.1–70.1	49.4–75.7
10	592.	12	42.2	39.2–46.9	39.1–49.0
15 measurements per bin ^b					
1	10.4	14	28.8	26.7–31.4	23.1–32.1
2	61.4	16	37.5	34.1–42.6	31.4–52.1
3	91.7	15	47.0	45.1–48.7	43.1–52.1
4	114.	15	56.0	54.9–60.0	53.0–70.1
5	139.	15	60.7	53.3–65.6	39.4–74.1
6	171.	14	72.8	67.1–78.4	65.4–83.7
7	216.	16	78.3	73.7–81.5	66.5–87.4
8	300.	15	70.7	59.2–78.0	52.8–114.
9	550.	15	42.6	39.2–48.0	39.1–51.1

^aMedian of ℓ_e values of measurements in the bin.

^bThe lower cutoffs on the integral of the likelihood function are 3, 0.1, 0.1, and 0.1 μK for 9, 11, 13, and 15 measurements per bin.

REFERENCES

- Amendola, L. 2001, *Phys. Rev. Lett.*, 86, 196
- Baker, J.C., et al. 1999, *MNRAS*, 308, 1173
- Balbi, A., et al. 2000, *ApJ*, 545, L1
- Balbi, A., Baccigalupi, C., Matarrese, S., Perrotta, F., & Vittorio, N. 2001, *ApJ*, 547, L89
- Barger, V., & Marfatia, D. 2001, *Phys. Lett. B*, 498, 67
- Barreiro, R.B. 2000, *New Astron. Rev.*, 44, 179
- Binétruy, P. 2000, *Int. J. Theo. Phys.*, 39, 1859
- Bond, J.R. 1995, *Phys. Rev. Lett.*, 74, 4369
- Bond, J.R., Jaffe, A.H., & Knox, L. 2000, *ApJ*, 533, 19
- Bunn, E.F., & Sugiyama, N. 1995, *ApJ*, 446, 49
- Carroll, S.M. 2000, *Living Rev. Relativity*, submitted
- Chimento, L.P., Jakubi, A.S., & Pavón, D. 2000, *Phys. Rev. D*, 62, 063508
- Coble, K., et al. 1999, *ApJ*, 519, L5
- de Bernardis, P., et al. 2000, *Nature*, 404, 955
- de Oliveira-Costa, A., Devlin, M.J., Herbig, T., Miller, A.D., Netterfield, C.B., Page, L.A., & Tegmark, M. 1998, *ApJ*, 509, L77
- Devlin, M.J., de Oliveira-Costa, A., Herbig, T., Miller, A.D., Netterfield, C.B., Page, L.A., & Tegmark, M. 1998, *ApJ*, 509, L69
- Dicker, S.R., et al. 1999, *MNRAS*, 309, 750
- Dodelson, S., & Knox, L. 2000, *Phys. Rev. Lett.*, 84, 3523
- Femenía, B., Rebolo, R., Gutiérrez, C.M., Limon, M., & Piccirillo, L. 1998, *ApJ*, 498, 117
- Ganga, K., Ratra, B., Church, S.E., Sugiyama, N., Ade, P.A.R., Holzzapfel, W.L., Mauskopf, P.D., & Lange, A.E. 1997b, *ApJ*, 484, 517
- Ganga, K., Ratra, B., Gundersen, J.O., & Sugiyama, N. 1997a, *ApJ*, 484, 7
- Ganga, K., Ratra, B., Lim, M.A., Sugiyama, N., & Tanaka, S.T. 1998, *ApJS*, 114, 165
- Ganga, K., Ratra, B., & Sugiyama, N. 1996, *ApJ*, 461, L61

- Gawiser, E., & Silk, J. 2000, *Phys. Rept.*, 333-334, 245
- González-Díaz, P.F. 2000, *Phys. Rev. D*, 62, 023513
- Górski, K.M. 1997, in *Microwave Background Anisotropies*, ed. F.R. Bouchet, R. Gispert, B. Guiderdoni, & J. Tran Thanh Van (Gif-sur-Yvette: Editions Frontières), 77
- Górski, K.M., Ratra, B., Stompor, R., Sugiyama, N., & Banday, A.J. 1998, *ApJS*, 114, 1
- Górski, K.M., Ratra, B., Sugiyama, N., & Banday, A.J. 1995, *ApJ*, 444, L65
- Gott, J.R. 1982, *Nature*, 295, 304
- Gott, J.R. 1997, in *Critical Dialogues in Cosmology*, ed. N. Turok (Singapore: World Scientific), 519
- Gott, J.R., Vogeley, M.S., Podariu, S., & Ratra, B. 2001, astro-ph/0006103, *ApJ*, 548, in press
- Gutiérrez, C.M., Rebolo, R., Watson, R.A., Davies, R.D., Jones, A.W., & Lasenby A.N. 2000, *ApJ*, 529, 47
- Haiman, Z., Mohr, J.J., & Holder, G.P. 2000, *ApJ*, submitted
- Hanany, S., et al. 2000, *ApJ*, 545, L5
- Harrison, D.L., et al. 2000 *MNRAS*, 316, L24
- Hebecker, A., & Wetterich, C. 2001, *Phys. Lett. B*, 497, 281
- Herbig, T., de Oliveira-Costa, A., Devlin, M.J., Miller, A.D., Page, L.A., & Tegmark, M. 1998, *ApJ*, 509, L73
- Hinshaw, G., Banday, A.J., Bennett, C.L., Górski, K.M., Kogut, A., Smoot, G.F., & Wright, E.L. 1996, *ApJ*, 464, L17
- Kamionkowski, M., Ratra, B., Spergel, D.N., & Sugiyama, N. 1994, *ApJ*, 434, L1
- Knox, L., & Page, L. 2000, *Phys. Rev. Lett.*, 85, 1366
- Kogut, A., Banday, A.J., Bennett, C.L., Górski, K.M., Hinshaw, G., Smoot, G.F., & Wright, E.L. 1996, *ApJ*, 464, L5
- Lange, A.E., et al. 2001, *Phys. Rev. D*, 63, 042001
- Le Dour, M., Douspis, M., Bartlett, J.G., & Blanchard, A. 2000, *A&A*, submitted
- Leitch, E.M., Readhead, A.C.S., Pearson, T.J., Myers, S.T., Gulkis, S., & Lawrence, C.R. 2000, *ApJ*, 532, 37

- Mauskopf, P.D., et al. 2000, *ApJ*, 536, L59
- Meinhold, P., et al. 1993, *ApJ*, 409, L1
- Miller, A.D., et al. 1999, *ApJ*, 524, L1
- Netterfield, C.B., Devlin, M.J., Jarosik, N., Page, L., & Wollack, E.J. 1997, *ApJ*, 474, 47
- Page, L.A.. 1997, in *Critical Dialogues in Cosmology*, ed. N. Turok (Singapore: World Scientific), 343
- Page, L.A. 1999, astro-ph/9911199
- Peebles, P.J.E. 1984, *ApJ*, 284, 439
- Peebles, P.J.E., & Ratra, B. 1988, *ApJ*, 325, L17
- Peterson, J.B., et al. 2000, *ApJ*, 532, L83
- Podariu, S., Nugent, P., & Ratra, B. 2001, astro-ph/0008281, *ApJ*, 553, in press
- Podariu, S., & Ratra, B. 2000, *ApJ*, 532, 109
- Ratra, B., Ganga, K., Stompor, R., Sugiyama, N., de Bernardis, P., & Górski, K.M. 1999a, *ApJ*, 510, 11
- Ratra, B., Ganga, K., Sugiyama, N., Tucker, G.S., Griffin, G.S., Nguyễn, H.T., & Peterson, J.B. 1998, *ApJ*, 505, 8
- Ratra, B., & Peebles, P.J.E. 1988, *Phys. Rev. D*, 37, 3406
- Ratra, B., & Peebles, P.J.E. 1994, *ApJ*, 432, L5
- Ratra, B., & Peebles, P.J.E. 1995, *Phys. Rev. D*, 52, 1837
- Ratra, B., Stompor, R., Ganga, K., Rocha, G., Sugiyama, N., & Górski, K.M. 1999b, *ApJ*, 517, 549
- Ratra, B., Sugiyama, N., Banday, A.J., & Górski, K.M. 1997, *ApJ*, 481, 22
- Rocha, G. 1999, in *Dark Matter in Astrophysics and Particle Physics 1998*, ed. H.V. Klapdor-Kleingrothaus & L. Baudis (Bristol: Institute of Physics Publishing), 238
- Rocha, G., Stompor, R., Ganga, K., Ratra, B., Platt, S.R., Sugiyama, N., & Górski, K.M. 1999, *ApJ*, 525, 1
- Sahni, V., & Starobinsky, A. 2000, *Int. J. Mod. Phys. D*, 9, 373
- Steinhardt, P.J. 1999, in *Proceedings of the Pritzker Symposium on the Status of Inflationary Cosmology*, in press

- Stompor, R. 1997, in *Microwave Background Anisotropies*, ed. F.R. Bouchet, R. Gispert, B. Guiderdoni, & J. Tran Thanh Van (Gif-sur-Yvette: Editions Frontières), 91
- Tegmark, M., & Zaldarriaga, M. 2000, *ApJ*, 544, 30
- Torbet, E., et al. 1999, *ApJ*, 521, L79
- Tucker, G.S., Gush, H.P., Halpern, M., Shinkoda, I., & Towlson, W. 1997, *ApJ*, 475, L73
- Tye, S.-H.H., & Wasserman, I. 2001, *Phys. Rev. Lett.*, 86, in press
- Wilson, G.W., et al. 2000, *ApJ*, 532, 57

FIGURE CAPTIONS

Fig. 1. – CMB anisotropy bandtemperature predictions and observational results, as a function of multipole ℓ . Colored hatched regions are adiabatic CDM model predictions for what would be seen by a series of ideal, Kronecker-delta window-function, experiments. (That is, the model predictions do not account for the experiment window functions.) These are for baryonic density parameter $\Omega_B = 0.0125h^{-2}$ (where the Hubble constant $H_0 = 100h \text{ km s}^{-1} \text{ Mpc}^{-1}$) and are normalized to the $\pm 1 \sigma$ range allowed by the DMR measurements (Górski et al. 1998; Stompor 1997). Green is a flat- Λ model with nonrelativistic matter density parameter $\Omega_0 = 0.4$ and $h = 0.6$, red is an open model with $\Omega_0 = 0.4$ and $h = 0.65$, and blue is fiducial CDM with $\Omega_0 = 1$ and $h = 0.5$. “Points” with different symbols represent observational results. Since most of the smaller-scale data points are derived assuming a flat bandpower CMB anisotropy angular spectrum, which is more accurate for narrower (in ℓ) window functions, we have shown the observational results from the narrowest windows available. Open symbols with inserted solid inverted triangles are 2σ upper limits. There are 37 2σ upper limits but 17 of these lie above $\delta T_\ell = 120 \mu\text{K}$ and so are not shown on the plot. (In those cases for which a proper 2σ upper limit has not been quoted by the observational group we have simply doubled the quoted 1σ upper error bar. Such approximate 2σ upper limits likely underestimate the true 2σ upper limits. Note that the two upper limits with $\delta T_\ell < 58 \mu\text{K}$ at $\ell \sim 400$ fall in to this category.) Detections have $\pm 1 \sigma$ vertical error bars. There are 142 detections but 2 of them (SK94Q9 and SK95C15) lie off the top of the plot. Horizontal “error bars” represent the width of the corresponding window functions. These data will eventually be available at www.phys.ksu.edu/~tarun/CMBwindows/wincomb/wincomb_tf.html. The data shown are from the DMR galactic frame maps ignoring the Galactic emission correction (Górski 1997, open octagons with $\ell \leq 20$); FIRS (Bond 1995, solid pentagon); Tenerife (Gutiérrez et al. 2000, open five-point star); Python I–III and V (Rocha et al. 1999 and T. Souradeep, private communication 2000, open six-point stars); BOOMERanG 1997 and 1998 (Mauskopf et al. 2000; de Bernardis et al. 2000, open four-point stars); IAC–Bartol (Femenía et al. 1998, open four-point diamond); Saskatoon 1993–95 (Netterfield et al. 1997, open squares); UCSB South Pole 1994 (Ganga et al. 1997a, solid circles); BAM (Tucker et al. 1997, open circle); MAT 1997 and 1998 (Torbet et al. 1999; Miller et al. 1999, open pentagons); MAXIMA-1 (Hanany et al. 2000, skeletal stars); QMAP 1 and 2 (Devlin et al. 1998; Herbig et al. 1998, solid pentagons); ARGO Hercules (Ratra et al. 1999a, solid square); Jodrell Bank–IAC (Dicker et al. 1999; Harrison et al. 2000, solid hexagons); Viper (Peterson et al. 2000, open seven-point stars); MAX3–5, (J. Gundersen, private communication, 1995; S. Tanaka private communication 1995; Ganga et al. 1998, open hexagons); MSAM combined (Wilson et al. 2000, solid four-sided diamonds); CAT 1 and 2 (G. Rocha, private communication, 1997; Baker et al. 1999, open four-sided diamonds); OVRO (Leitch et al. 2000, open five-point star); and White Dish (Ratra et al. 1998, open pentagon).

Fig. 2. – CMB anisotropy bandtemperature predictions (colored hatched regions — models are de-

scribed in the caption of Figure 1), binned weighted-mean observational detection data for all 142 measurements (solid black points connected by a solid black line are the central values and the other four solid black lines are the $\pm 1 \sigma$ and $\pm 2 \sigma$ limits), 10 times the number of standard deviations the weighted-mean result deviates from what is expected on the basis of Gaussianity of the CMB anisotropy (dashed line), and observational 2σ upper limits, all as a function of multipole ℓ . Note that the model predictions here (and in subsequent figures) have not been processed in the same manner as the observational data. This is because the window functions of some experiments are not available.

Fig. 3. – CMB anisotropy bandtemperature predictions (colored hatched regions — models are described in the caption of Figure 1), binned median-statistics observational detection data for all 142 measurements (solid black points connected by a solid black line are the central values and the other four solid black lines are the $\pm 1 \sigma$ and $\pm 2 \sigma$ limits), and observational 2σ upper limits, all as a function of multipole ℓ .

Fig. 4. – CMB anisotropy bandtemperature predictions (colored hatched regions — models are described in the caption of Figure 1), binned weighted-mean observational detection data for the culled data with 135 measurements (solid black points connected by a solid black line are the central values and the other four solid black lines are the $\pm 1 \sigma$ and $\pm 2 \sigma$ limits), 10 times the number of standard deviations the weighted-mean result deviates from what is expected on the basis of Gaussianity of the CMB anisotropy (dashed line), and observational 2σ upper limits, all as a function of multipole ℓ .

Fig. 5. – CMB anisotropy bandtemperature predictions (colored hatched regions — models are described in the caption of Figure 1), binned median-statistics observational detection data for the culled data with 135 measurements (solid black points connected by a solid black line are the central values and the other four solid black lines are the $\pm 1 \sigma$ and $\pm 2 \sigma$ limits), and observational 2σ upper limits, all as a function of multipole ℓ .

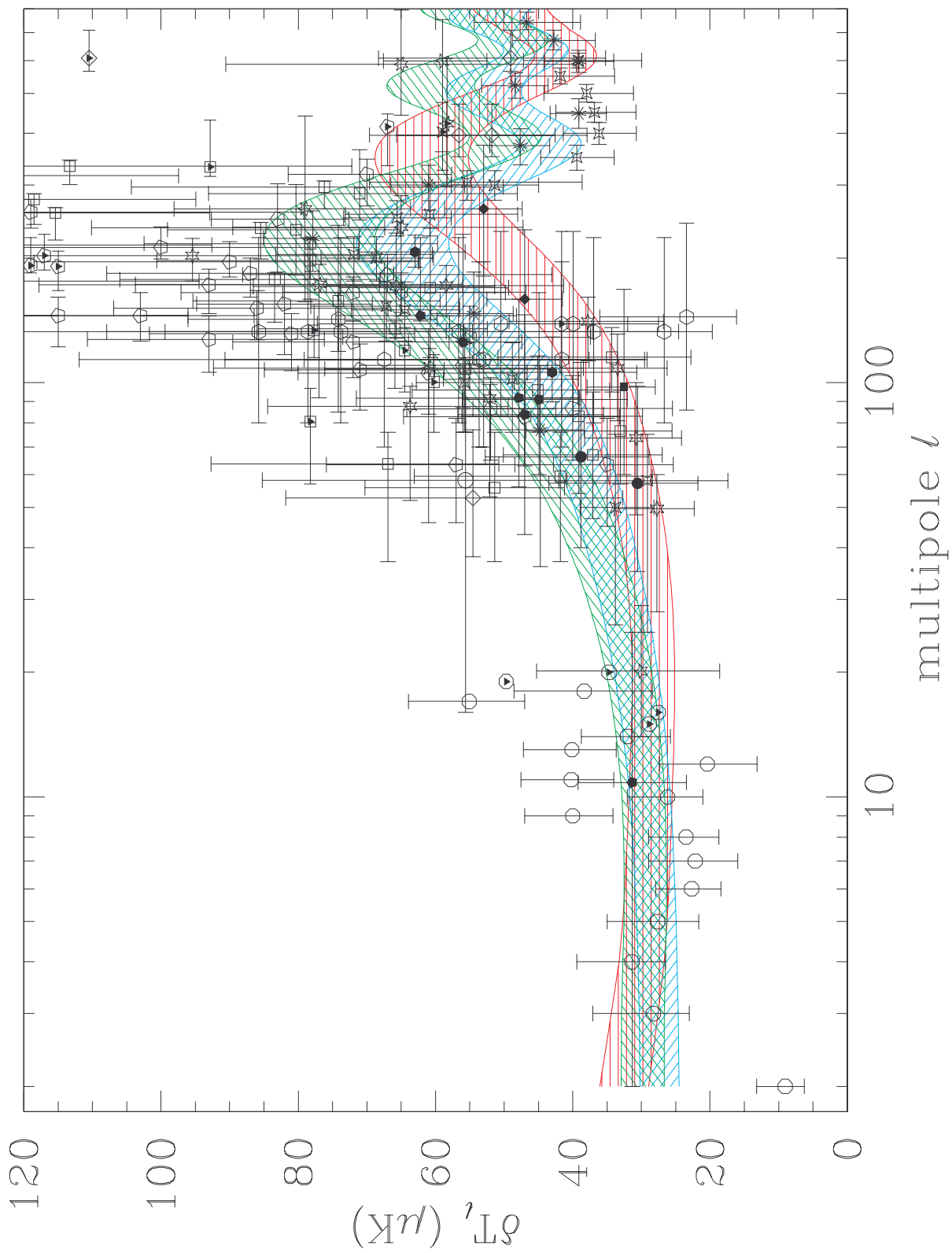


Figure 1

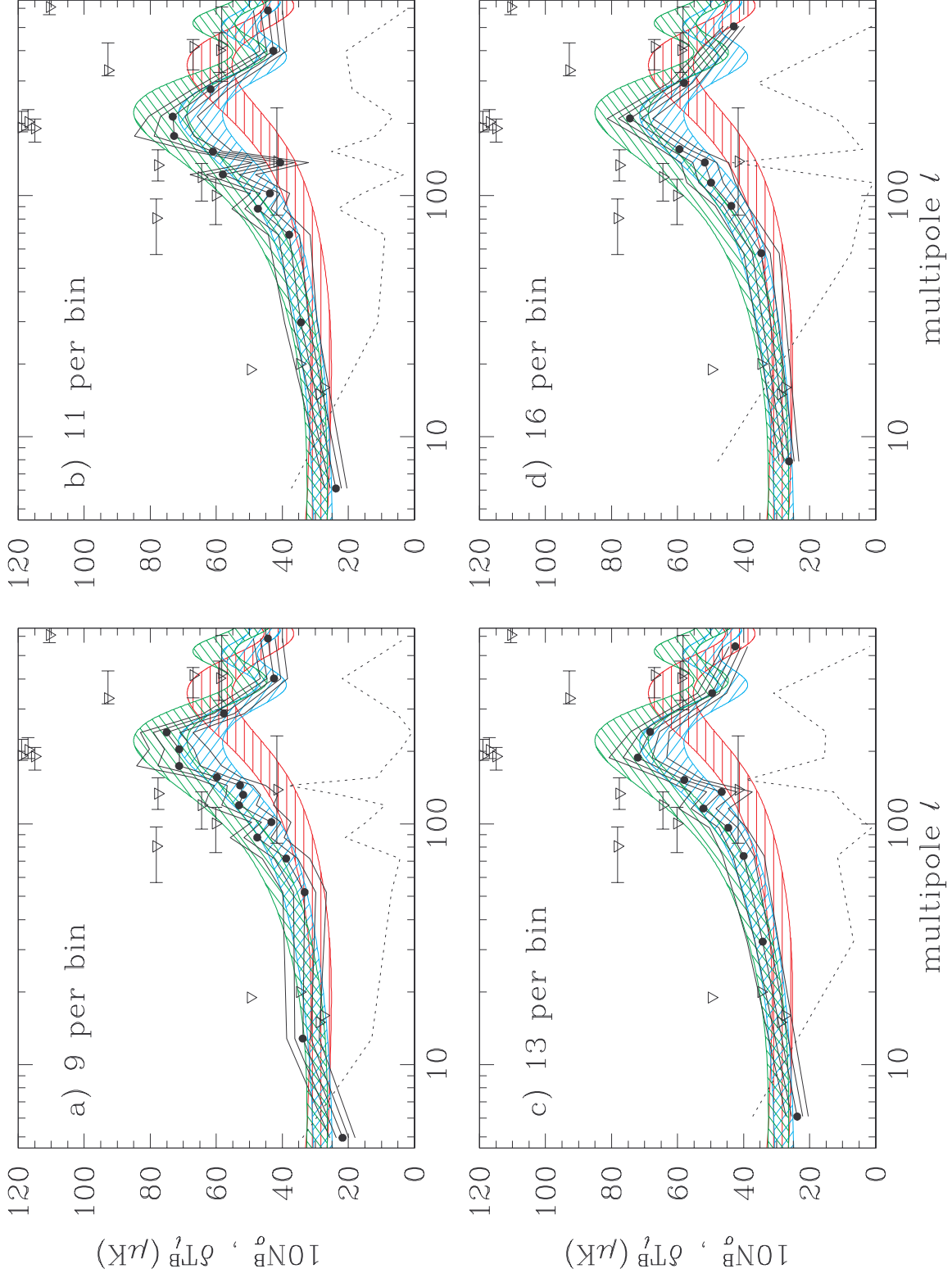


Figure 2

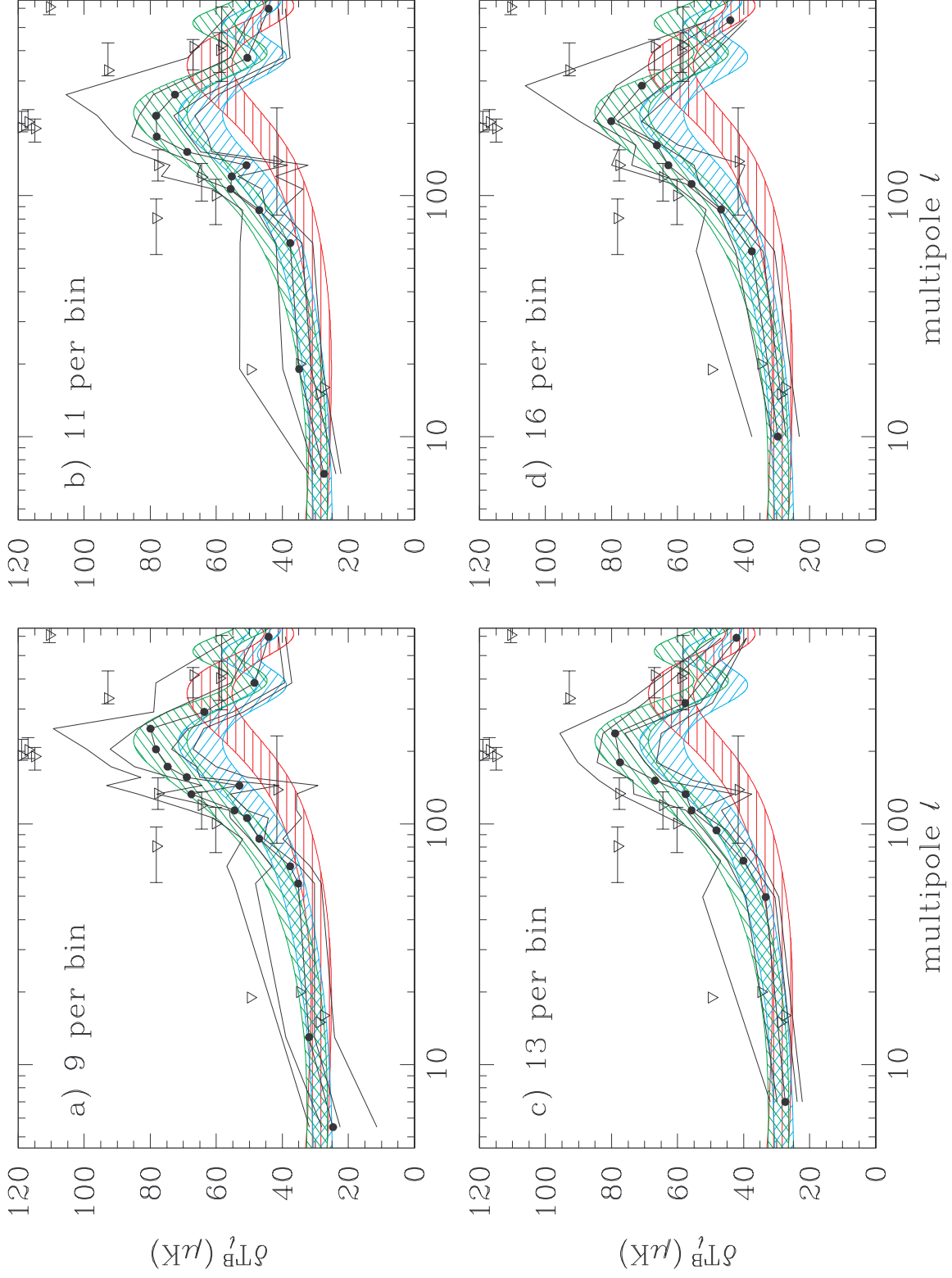


Figure 3

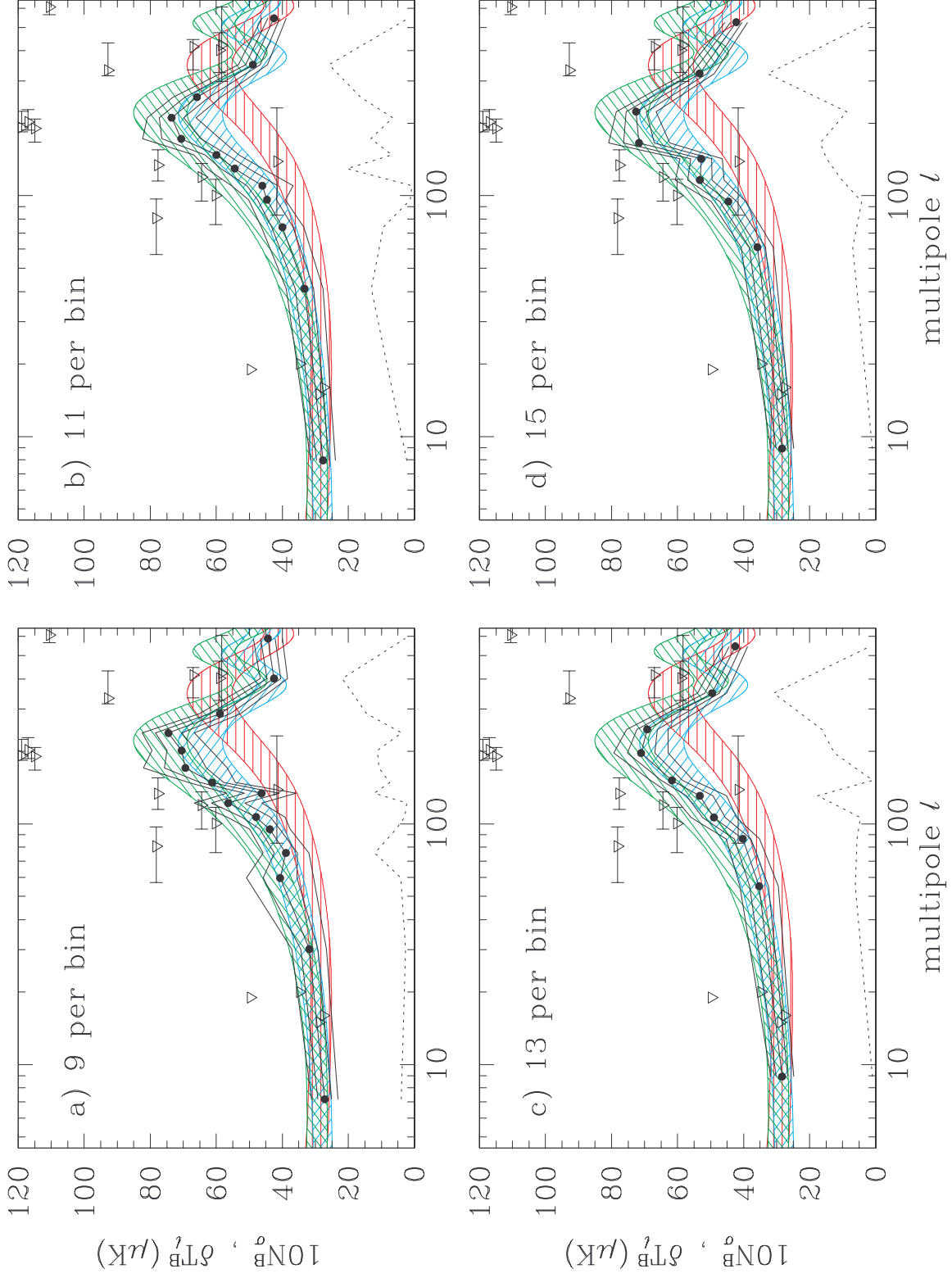


Figure 4

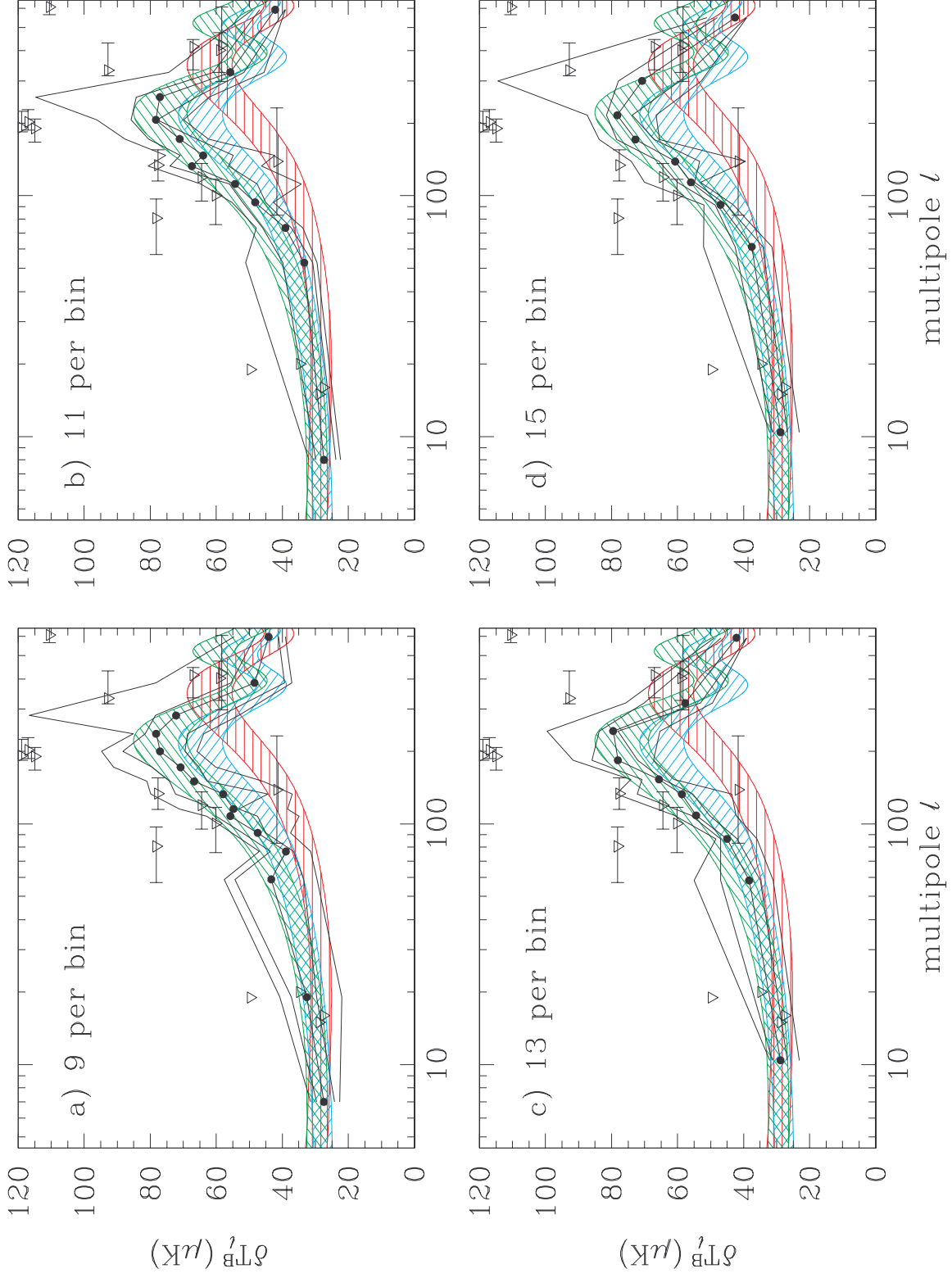


Figure 5